JITH 2017
18èmes Journées Internationales de Thermique (JITH 2017)
Monastir (Tunisie), 25 - 27 Octobre 2017

Numerical investigation of phase change material melting in slabs heated by upward or downward heat transfer fluid flow

[1]Radouane ELBAHJAOUI, [1]Hamid EL QARNIA and [2]Mohammed EL GANAOUI

[1]Cadi Ayyad University, Faculty of Sciences Semlalia, Department of Physics, P.O 2390,
Fluid Mechanics and Energetic Laboratory, Marrakesh, Morocco
[2]Université de Lorraine, Laboratoire d'Energétique de Longwy, (FJV/LERMAB), Institut Henri Poincaré, de Longwy, France

elqarnia@uca.ac.ma; radouane.elbahjaoui@ced.uca.ac.ma

Abstract: The present work aims to numerically investigate the thermal and flow characteristics of a rectangular latent heat storage unit (LHSU) during the melting process of a phase change material (PCM). The LHSU consists of a number of vertical and identical slabs of phase change material (PCM) separated by rectangular channels. The melting process is initiated when the LHSU is heated by a heat transfer fluid (HTF: water) flowing in channels in downward or upward direction. The proposed study is motivated by the need to optimize the thermal performance of latent heat storage units by accelerating the charging process in solar thermal storage applications. A mathematical model is developed and a fixed-grid enthalpy formulation is adopted for modeling the melting process. The finite volume method was used for discretization. The obtained numerical results are compared with experimental, analytical and numerical ones found in the literature and a reasonably good agreement is obtained. Thereafter, the numerical investigations were carried out to highlight the effects of the HTF flow direction and Reynolds number on the heat transfer enhancement and thermal performance of the storage unit.

Keywords: phase change material (PCM), latent heat storage unit (LHSU), heat transfer fluid (HTF), solar thermal energy storage, melting.

1. Introduction

Due to the gap between the thermal energy production and utilization, latent heat storage units (LHU) are considered as attractive thermal systems to conserving available energy. These systems integrate phase change materials (PCMs) which are characterized by a relatively high energy storage density (compared to materials storing energy by sensible form) and a small swing temperature during phase transition. These two characteristics are advantageous for latent heat storage applications due to their role in reducing the volume of storing materials without appreciable variation of the temperature around the melting point. LHSU were the subject of numerous research works during the last 20 years. This interest is due to the fact that they are used in several practical applications including solar building systems [1, 2], solar water heating systems [3, 4] and solar energy generation systems [5-9].

Charvát et al. [10] reported experimental and numerical investigation of a heat storage unit containing 100 aluminum panels filled with phase change material (PCM) and 20 mm air gap (air channel) between the panels. A 1D mathematical model was developed and used for a parametric study. Mosaffa et al. [11] numerically studied the performance enhancement of a thermal energy storage (TES) unit employing multiple PCMs and using the effective heat capacity method. The storage unit is composed of a number of horizontal PCMs slabs separated by rectangular channels through which a heat transfer fluid (HTF) flows. The effects of the PCM slabs dimension and HTF channel gap on the storage performance were numerically investigated. The results show that the optimum length is 1.3 m, the slab thickness is 10 mm and the air channel gap is 3.2 mm. The results also show that the system which can ensure comfort conditions has approximately a COP of 7.0 in the climate of Tabriz (Iran). Bechiri and Mansouri [12] analytically investigated the thermal performance of a

latent heat storage unit (LHSU) composed of various PCM flat slabs heated by HTF flowing under laminar forced convection. The results show that the obtained exact solution gives a good estimation of the thermal behavior of the LHSU during charging and discharging processes. Lopez et al. [13] developed a numerical model taking into account conduction in PCM and heat transfer between the airflow and the PCM plates for thermal energy storage in buildings. Halawa and Saman [14] carried out a numerical study of an air LHSU used for space heating. The LHSU consists of one dimensional rectangular ducts filled with phase change material (PCM) where the heat transfer fluid (HTF) flows between the PCM slabs. The effects of the design parameters such as air mass flow rate, air gaps, slab dimension and charge/discharge temperatures differences on the heat transfer rate and air outlet temperature have been investigated. Ye et al. [15] numerically studied the melting of PCM not completely filled inside the enclosures on the heat transfer and fluid flow characteristics. They investigated the time required for the complete storage, the volume expansion ratio, liquid fraction, heat flux, velocity and temperature fields for a range of cavity volume fractions of PCM between 35% and 95%. The computational results indicate that the time required for the complete energy storage increases with the increase of the PCM cavity volume fraction. Gharebaghi and Sezai [16] performed a numerical study of the thermal performance of a LHSU composed of slabs containing paraffin as PCM and metal fins where a HTF (air) flows in the gap between the PCM modules. The results show that the heat transfer rate to PCM can be enhanced by adding fins. Borderon et al. [17] modeled a storage system integrated in the ventilation circuit and composed of horizontal phase change material sheets placed in a box beam where air blows between the sheets and exchanges heat by convection with PCM. Lazaro et al. [18] experimentally studied a phase change thermal storage system used for free-cooling. In this application, PCM is solidified during the night and then during the day, the inside air of a building can became cold by exchanging heat with PCM. El Qarnia [19] numerically studied the transient behavior of a latent heat thermal energy storage (LHTES) system composed of a number of PCM slabs separated by rectangular channels where a HTF flows and exchanges heat by forced convection with PCM. The author investigated the effects of control parameters on the thermal performance and behavior of the LHTES system. Ait Adine and El Qarnia [20] numerically studied the thermal performance of a LHSU using single and various phase change materials (PCMs). The results show that, for a low mass flow rate and HTF inlet temperature, high thermal storage efficiency is obtained for a LHSU using two PCMs. Prieto and González [21] studied the fluid flow and heat transfer during melting and solidification of PCM filled inside vertical and horizontal arranged rectangular panels. They evaluated the effect of the walls temperature, position and thickness of PCM panels on the flow behavior for two kinds of PCM (RT60 and Palmitic acid). The results show that during melting process, the natural convection becomes more important for a horizontal arrangement of PCM panels. Bechiri and Mansouri [22] conducted an analytical study to investigate the thermal behavior of a shell-and-tube LHSU by using the variables separation technique and the exponential integration functions. They also examined the effects of the HTF mass flow rate, outer tube radius and pipe length on the melting and solidification rates. Elbahjaoui et al. [23, 24] numerically investigated the effect of the dispersion of high conductive alumina nanoparticles in a base PCM on the thermal performance and flow characteristics of a rectangular LHSU during melting process. The storage unit consists of a number of vertical and identical slabs filled with nanoparticle-enhanced phase change material (NEPCM) separated by rectangular channels in which circulates water as a HTF. The results reveal that the dispersion of high conductive nanoparticles reduces the PCM melting time. The results also show that the increase in the volumetric fraction of nanoparticles improves the thermal storage by sensible heat and slightly affects the latent heat storage.

In most of rectangular latent heat storage systems heated by HTF flows mentioned previously, the PCM plates are placed in horizontally arrangement. In addition, the effect of natural convection is not taken into account and can be neglected as reported by Laouadi and Lacroix [25]. The proposed work overcomes this limitation by taking into consideration the effect of natural convection during the melting process of PCM (Paraffin wax P116) filled in vertical slabs composing a LHSU. Because the melting process is initiated by the circulation of heat transfer fluid (water) between the PCM slabs, the effect of the flow direction (downward and upward flows) is also taken into consideration. The objective of this study is to investigate the effect of the HTF flow direction in channels and Reynolds number on the thermal and flow characteristics of the LHSU.

2. Mathematical model and validation

2.1. Configuration description

A schematic of the latent heat storage unit (LHSU) under investigation is shown in Fig. 1a. It consists of a number of PCM slabs separated by N rectangular channels through which HTF flows. A representative volume in the LHSU, which is repetitive, is chosen. The solution domain is shown in Fig. 1b. It consists of half a PCM slab and half a HTF channel. The PCM and HTF used are paraffin wax P116 and water, respectively. At time t = 0, the PCM is solid at its melting temperature, T_{melt}. The melting process of PCM is initiated, at t > 0, when HTF (hot water) flows in channels. The phase change process continues until all the PCM becomes completely melted and when its temperature becomes equal to that of HTF at the inlet of the LHSU.

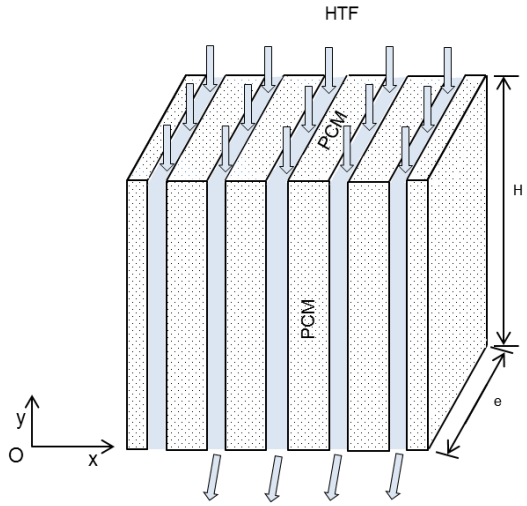

Figure 1a: Latent heat storage unit (LHSU)

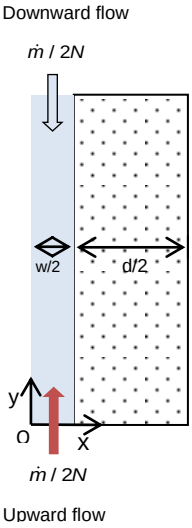

Figure 1b: Computational domain

2.2. Governing equations

In order to model the heat transfer by natural convection and conduction in PCM and by forced convection in HTF, some assumptions are adopted. It is assumed that the transient heat transfer and fluid flow are two-dimensional. The PCM is assumed to be pure, homogeneous and isotropic. The thermo-physical properties of HTF and PCM, which are provided in Tables 1 and 2, are assumed to be constant. The liquid PCM and HTF are Newtonian and incompressible and their flows are laminar. The HTF flow is dynamically developed. The Boussinesq approximation is valid for the PCM liquid phase density variations in the buoyancy source term. Viscous dissipation is neglected. The wall separating HTF and PCM is assumed to be very thin, so its thermal resistance is neglected. The contact between PCM and wall is perfect and permanent. The solid PCM is immobilized. The reference temperature, $T_{ref} = T_{melt}$, and the reference density, $\rho_{ref} = \rho\ (T = T_{melt})$, are made to the melting point.

Based on the previous simplifying assumptions and using the enthalpy method, the unsteady two dimensional governing equations for conservation of mass, momentum and energy are written as follows:

For PCM:

Continuity equation:

$$\frac{\partial U_m}{\partial X} + \frac{\partial V_m}{\partial Y} = 0 \tag{1}$$

Momentum equations

$$\frac{\partial U_m}{\partial \tau} + \frac{\partial U_m U_m}{\partial X} + \frac{\partial V_m U_m}{\partial Y} = -\frac{\partial P}{\partial X} + \frac{\partial}{\partial X}\left(Pr \frac{\partial U_m}{\partial X}\right) + \frac{\partial}{\partial Y}\left(Pr \frac{\partial U_m}{\partial Y}\right) - \bar{C}\frac{(1-f)^3}{(f^3+b)} U_m \tag{2a}$$

$$\frac{\partial V_m}{\partial \tau} + \frac{\partial U_m V_m}{\partial X} + \frac{\partial V_m V_m}{\partial Y} = -\frac{\partial P}{\partial Y} + \frac{\partial}{\partial X}\left(Pr \frac{\partial V_m}{\partial X}\right) + \frac{\partial}{\partial Y}\left(Pr \frac{\partial V_m}{\partial Y}\right) - \bar{C}\frac{(1-f)^3}{(f^3+b)} V_m + Ra\, Pr\, \theta_m \tag{2b}$$

Energy equation

$$\frac{\partial(\theta_m)}{\partial \tau} + \frac{\partial(U_m \theta_m)}{\partial X} + \frac{\partial(V_m \theta_m)}{\partial Y} = \frac{\partial}{\partial X}\left(\bar{\alpha}_m \frac{\partial \theta_m}{\partial X}\right) + \frac{\partial}{\partial Y}\left(\bar{\alpha}_m \frac{\partial \theta_m}{\partial Y}\right) - \frac{1}{Ste}\frac{\partial f}{\partial \tau} \tag{3}$$

For HTF (in downward flow):

$$\frac{\partial \theta_f}{\partial \tau} + \frac{\partial(V_f \theta_f)}{\partial Y} = \frac{\partial}{\partial X}\left(\bar{\alpha}_f \frac{\partial \theta_f}{\partial X}\right) + \frac{\partial}{\partial Y}\left(\bar{\alpha}_f \frac{\partial \theta_f}{\partial Y}\right) \tag{4}$$

where,

$$V_f = \frac{3}{2} Pr_f\, \bar{\alpha}_f\, \frac{Re}{\bar{D}_h}\left(1 - \left(\frac{X}{\bar{w}/2}\right)^2\right) \tag{5a}$$

$$\bar{\alpha}_m = \frac{\alpha_m}{\alpha_{m,l}} = f + (1-f)\bar{k}_{m,s}, \bar{\alpha}_f = \frac{\alpha_f}{\alpha_{m,l}} \text{ and } \bar{D}_h = 2\bar{w} \tag{5b}$$

The initial and boundary conditions for the conservation equations are as follows:

$$\tau = 0 \quad \theta_m = \theta_f = 0,\ U_m = V_m = 0 \tag{6a}$$

$$X = 0 \quad \frac{\partial \theta_f}{\partial X} = 0 \tag{6b}$$

$$Y = 0 \quad \frac{\partial \theta_m}{\partial Y} = \frac{\partial \theta_f}{\partial Y} = 0,\ U_m = V_m = 0 \tag{6c}$$

$$X = \bar{w}/2 \quad \bar{k}_m \frac{\partial \theta_m}{\partial X} = \bar{k}_f \frac{\partial \theta_f}{\partial X},\ U_m = V_m = 0 \tag{6d}$$

$$X = \bar{w}/2 + \bar{d}/2 \quad \frac{\partial \theta_m}{\partial Y} = 0,\ U_m = 0, \frac{\partial V_m}{\partial X} = 0 \tag{6e}$$

$$Y = \bar{H} \quad \frac{\partial \theta_m}{\partial Y} = 0,\ \theta_f = 1,\ U_m = V_m = 0 \tag{6f}$$

The dimensionless of the governing equations was obtained using the following dimensionless variables and parameters:

$$X = \frac{x}{l_0}, Y = \frac{y}{l_0}, \tau = \frac{\alpha_{m,l}\, t}{l_0^{\,2}}, U = \frac{u}{\alpha_{m,l}/l_0}, V = \frac{v}{\alpha_{m,l}/l_0}, \theta = \frac{T - T_{melt}}{T_{f,e} - T_{melt}},$$
$$Ra = \frac{g\beta_m\, l_0^{\,3}(T_{f,e} - T_{melt})}{\nu_m \alpha_{m,l}},\ Pr = \frac{\nu_m}{\alpha_{m,l}}, P = \frac{p}{\rho_m(\alpha_{m,l}/l_0)^2}, \bar{\alpha} = \frac{\alpha}{\alpha_{m,l}}, Ste = \frac{c_m(T_{f,e} - T_{melt})}{\Delta H_m}, \tag{7}$$
$$\bar{w} = \frac{w}{l_0},\ \bar{d} = \frac{d}{l_0},\ \bar{H} = \frac{H}{l_0},\ \bar{k}_f = \frac{k_f}{k_{m,l}} \text{ and } \bar{k}_m = \frac{k_m}{k_{m,l}}$$

where $T_{f,e}$ stands for the HTF inlet temperature, T_{melt} represents the PCM melting point, Ra is the Rayleigh number, Ste is the Stefan number and l_0 is a characteristic length ($l_0 = \sqrt{H(d/2)}$). It should be noted that the characteristic length is kept constant in the present study at value $l_0 = 0.07062$ m. The dimensionless height and thickness of the PCM slabs are expressed as a function of the aspect ratio as follows:

$$\bar{H} = \sqrt{A} \tag{8a}$$

$$\bar{d} = \frac{2}{\sqrt{A}} \tag{8b}$$

2.3. Numerical procedure and validation

The governing equations are discretized using the finite volume approach. The power law scheme is adopted to treat the convective terms in governing equations. The pressure-velocity coupling in momentum equations is handled using the SIMPLE algorithm. The Tri-diagonal Matrix Algorithm (TDMA) is used for solving the resulting algebraic equations.

The numerical model is implemented in a self-developed FORTRAN code to carry out the calculations. The iterative solution continues until convergence of the flow and temperature fields at each time step. Solution was declared converged when the largest local relative change in temperature is less than 10^{-6}, and when the largest mass and thermal balances are less than 10^{-8} and 5×10^{-3}, respectively.

In order to test the reliability of the foregoing mathematical model and self-developed simulation code, a comparison between our numerical results and analytical, experimental and numerical results obtained by other researchers has been made. Three validations have been carried out.

In the first validation, the problem of heat transfer by forced convection for a fluid flow between two parallel flat plates is studied. Two kinds of boundary conditions are considered, isothermal wall and constant heat flux density wall. According to the literature [26] , for fully thermal developed flow, the Nusselt numbers associated to an isothermal wall and constant heat flux density wall are 7.54 and 8.23, respectively. As it can be seen in Fig. 2 (a) and (b) which displays the variation of the Nusselt number with the position, the Nusselt number decreases from the inlet to the outlet of HTF channel for the both boundary cases. These results show that the Nusselt number reaches the asymptotic values 8.23 and 7.54 for a constant heat flux density wall and an isothermal wall, respectively. These obtained results are in agreement with those reported in literature.

In the second validation, the results obtained by the present numerical model are compared with those of the numerical studies of Brent et al. [27] and Khodadadi and Hosseinizadeh [28], and with the experimental

work of Gau and Viskanta [29] for the melting of gallium as a base PCM filled in a differentially heated rectangular enclosure. The height and width of the enclosure are 6.35 cm and 9.89 cm, respectively. The temperatures of the left and right walls are kept fixed at 38 °C and 28.3 °C, respectively. The horizontal walls of the enclosure are thermally insulated. The locations of the melting front at $t = 2$ min, 6 min, 10 min and 17 min predicted by the current model were compared with those obtained by Brent, Voller and Reid [27], Khodadadi and Hosseinizadeh [28] and Gau and Viskanta [29] as shown in Fig. 3. From this figure, it can be seen a reasonably agreement between the numerical and experimental results.

The third validation was carried out by comparing the results of the current model with the data of a benchmark study performed by Bertrand et al. [30] for the melting of PCM in a differentially heated square enclosure. The latter is initially filled with solid octadecane at the melting point. The right wall of the enclosure is fixed at the melting point, while the left vertical wall is maintained at 10°C higher than the melting temperature. The horizontal walls are thermally insulated. The results predicted by the current model were compared with the numerical models of "Lacroix", "LeQuere", "Gobin-Viera" and "Binet-Lacroix" for the melting front positions at times $\mathrm{Ste} \times \mathrm{Fo} = 0.006$ and 0.01 as shown in Fig. 4(a) and (b), respectively. The analysis of these results reveals that a good agreement exists between the current developed model and the other numerical models of "Lacroix", "LeQuere", "Gobin-Viera" and "Binet-Lacroix" [30].

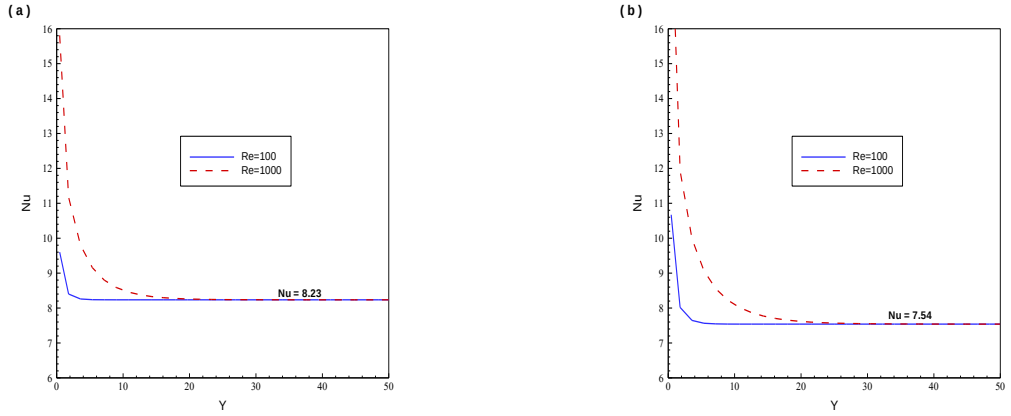

Figure 2: Local Nusselt number at thermally developing flow between parallel flat plates with (a) constant heat flux and (b) isothermal wall

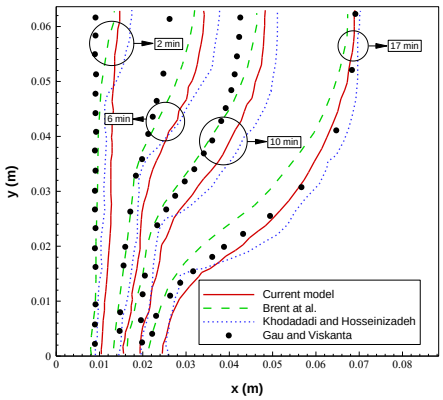

Figure 3: Comparison of the Gallium melting front positions at 2 min, 6 min, 10 min and 17 min between the current model and the numerical predictions of Brent, Voller and Reid [27] and Khodadadi and Hosseinizadeh [28] ,and experimental data of Gau and Viskanta [29]

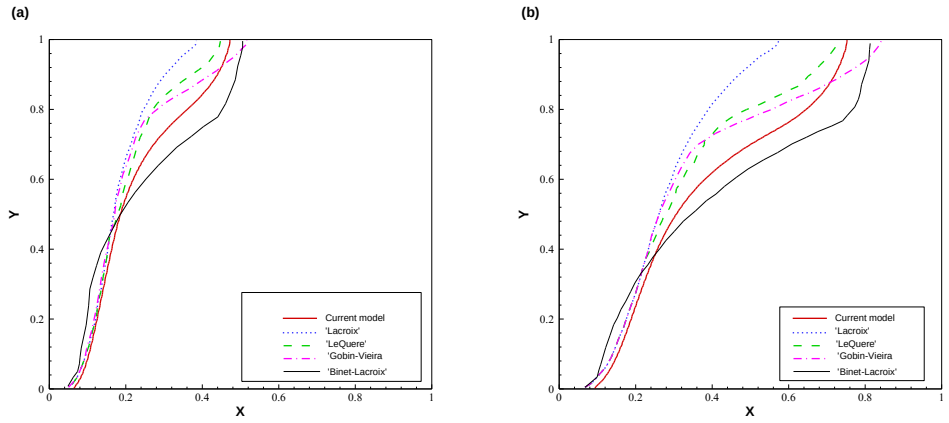

Figure 4: Comparison of the melting front positions at time Ste×Fo = 0.006 (a) and 0.01 (b) between the current model and the numerical models [30] of Lacroix, LeQuere, Gobin-Viera and Binet-Lacroix.

3. Results and discussions

This section focuses on the effects of the HTF flow direction (upward or downward direction) and Reynolds number on the flow and thermal characteristics of the LHSU during the melting process. The Reynolds number ranges from 40 to 2000. The aspect ratio, Rayleigh number and Stefan number are fixed at values: $A = 6$, $Ra = 7.95\times10^{7}$ and $Ste = 0.1444$, respectively. The other control parameters are fixed at their reference values as follows: $\bar{\alpha}_f = 1.3$, $\bar{w} = 0.085$, $Pr_f = 3.77$, $\bar{k}_{m,s} = 1.4916$ and $Pr_m = 19.87$.

To compare the thermal behavior and performance of the LHSU heated by a downward and an upward HTF flow, two different storage efficiencies were defined. The first efficiency, called sensible storage efficiency, is associated to the storage of energy by sensible heat. It is defined as the ratio between the sensible energy stored in the PCM and the maximum energy that can be stored. It is given as follows:

$$\varepsilon_{sen} = \frac{Ste \int_{X=\bar{w}/2}^{\bar{w}/2+\bar{d}/2} \int_{Y=0}^{\bar{H}} \theta_m dX\, dY}{1+Ste} \tag{9}$$

The second efficiency, called latent storage efficiency, concerns the storage of energy by latent heat. It is defined as the ratio between the energy stored by latent heat and the maximum energy that can be stored in PCM. It is expressed as follows

$$\varepsilon_{lat} = \frac{f}{1+Ste} \tag{10}$$

The latent storage efficiency, ε_{lat}, achieves its maximum value when the PCM becomes completely melted (f = 1). This maximum value, as can be concluded from the latest expression, is lower than the value 1. The sensible storage efficiency, ε_{sen}, reaches its maximum value when the thermal equilibrium establishes between PCM and HTF. At this moment, the PCM is heated up to the HTF inlet temperature and the sum of these two storage efficiencies becomes equal to 1 ($\varepsilon_{sen} + \varepsilon_{lat} = 1$).

3.1. Effect of the HTF flow direction on streamlines and isotherms

Fig. 5 shows the streamlines describing the flow field in the liquid PCM for an upward HTF flow at times: $\tau = 5.45\times10^{-2}$, 7.46×10^{-2}, 9.466×10^{-2}, 1.162×10^{-1}, 1.377×10^{-1}, 1.65×10^{-1}, 1.98×10^{-1} and 2.8×10^{-1}. The case of downward HTF flow is also investigated as illustrated in Fig. 6. The Reynolds number is fixed at value of 40. These figures show that a part of heat is transmitted to PCM and thereby causes its melting startup for both cases, upward and downward flow of HTF. The natural convection begins to develop near the heat exchange wall separated HTF and PCM. The liquid PCM flow is in the clockwise direction, upward close to the heated wall and downward near the melting front. As can be seen in Figs. 5(a) - 5(d), the liquid PCM flow is mono-cellular where a single cell is formed in the melted portion. The heated liquid moves to the top part of the PCM slab before impinging on the melting front. The displacement of the hot liquid PCM toward the top of the slab causes an accelerated melting in this region. This causes the deformation and rapid progression of the melting front in this section of PCM slab. Compared to the case of an upward HTF flow, the melt front is deformed more quickly in the upper part of the PCM slab for a downward HTF flow. As time progresses, the liquid volume widens, and

the effect of natural convection intensifies. For $\tau = 1.377\times10^{-1}$, the liquid PCM flow becomes bi-cellular for an upward HTF flow, while it remains mono-cellular for a downward flow of HTF. As heating ongoing ($\tau = 2.8\times10^{-1}$) the liquid PCM region becomes more extended and the both cells previously formed, for the case of an upward HTF flow, combines together to form a single clockwise cell. It is interesting to note that at the same moment, the liquid PCM flow is more intensified for the case of an upward HTF. This behavior is represented in Fig. 5 and Fig. 6 by the great value of $|\Psi|_{max}$ for an upward HTF flow compared to a downward flow.

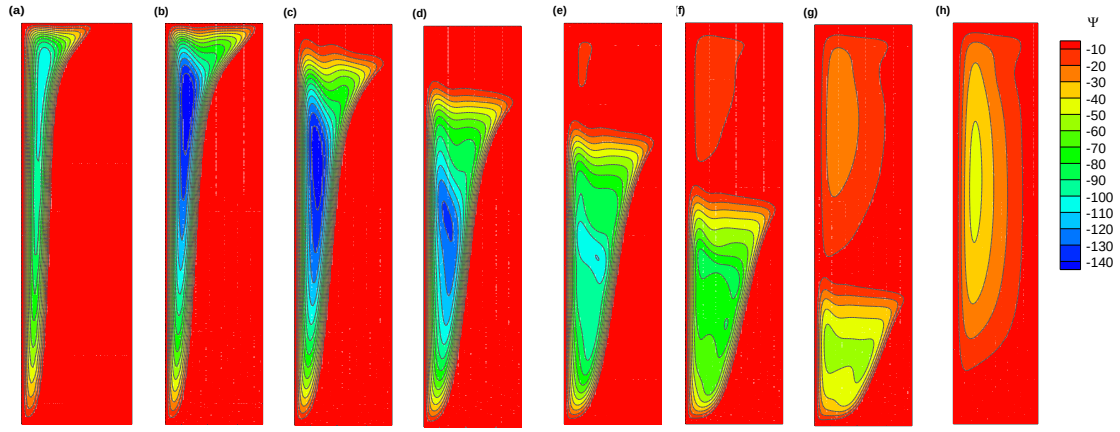

Figure 5: Streamlines for an upward HTF flow at (a) $\tau = 5.45\times10^{-2}$, (b) 7.46×10^{-2}, (c) 9.466×10^{-2}, (d) 1.162×10^{-1}, (e) 1.377×10^{-1}, (f) 1.65×10^{-1}, (g) 1.98×10^{-1} and (h) 2.8×10^{-1}

Fig.7 shows the temperature contours in the PCM slabs, for an upward HTF flow, at the same aforementioned times: $\tau = 5.45\times10^{-2}$, 7.46×10^{-2}, 9.466×10^{-2}, 1.162×10^{-1}, 1.377×10^{-1}, 1.65×10^{-1}, 1.98×10^{-1} and 2.8×10^{-1}. The case of downward HTF is also treated as illustrated in Fig. 8. Figs. 7 and 8 show that, for both cases of HTF flow direction (upward or downward flow), the melted PCM close to the heated wall moves towards the top region of the enclosure as melting progresses. Such a movement is due to natural convection occurring inside the melted PCM. As a consequence, a non-uniform temperature distribution occurs in the vertical direction. It should be noted that, for both cases of HTF flow direction, the highest temperature takes place in the top region of PCM slabs. It is interesting to note that compared to the temperature distribution in PCM slab for an upward HTF flow, the highest value of temperature is achieved for a downward flow of HTF.

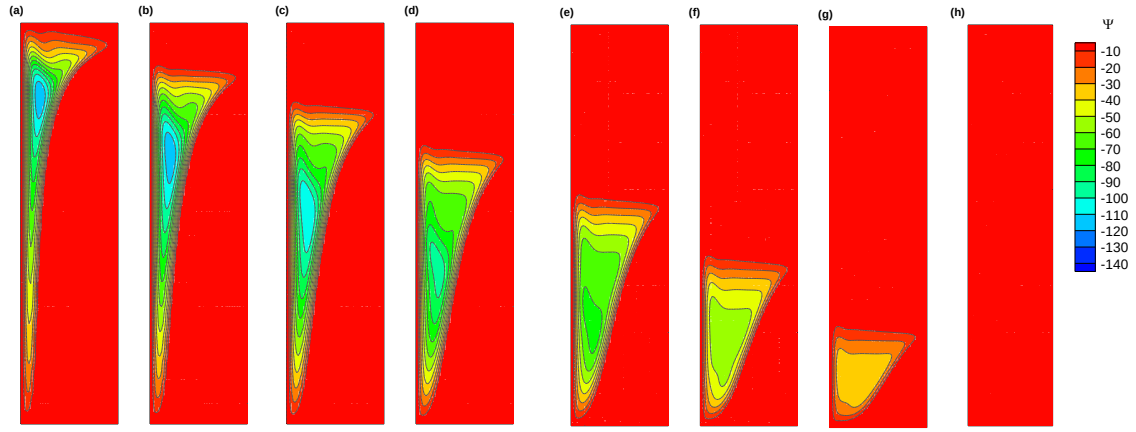

Figure 6: Streamlines for a downward HTF flow in channels at (a) $\tau = 5.45\times10^{-2}$, (b) 7.46×10^{-2}, (c) 9.466×10^{-2}, (d) 1.162×10^{-1}, (e) 1.377×10^{-1}, (f) 1.65×10^{-1}, (g) 1.98×10^{-1} and (h) 2.8×10^{-1}

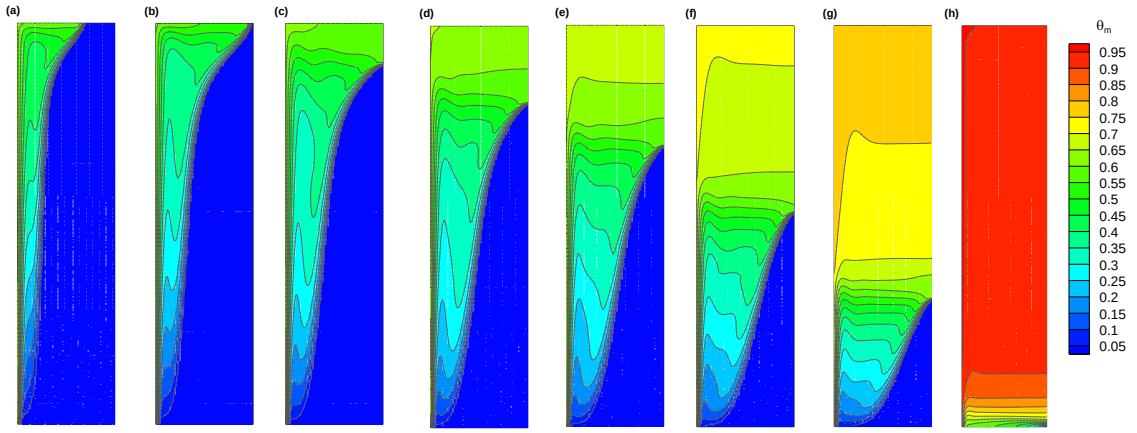

Figure 7:Isotherms for an upward HTF flow in channels at (a) $\tau = 5.45\times10^{-2}$, (b) 7.46×10^{-2}, (c) 9.466×10^{-2}, (d) 1.162×10^{-1}, (e) 1.377×10^{-1}, (f) 1.65×10^{-1}, (g) 1.98×10^{-1} and (h) 2.8×10^{-1}

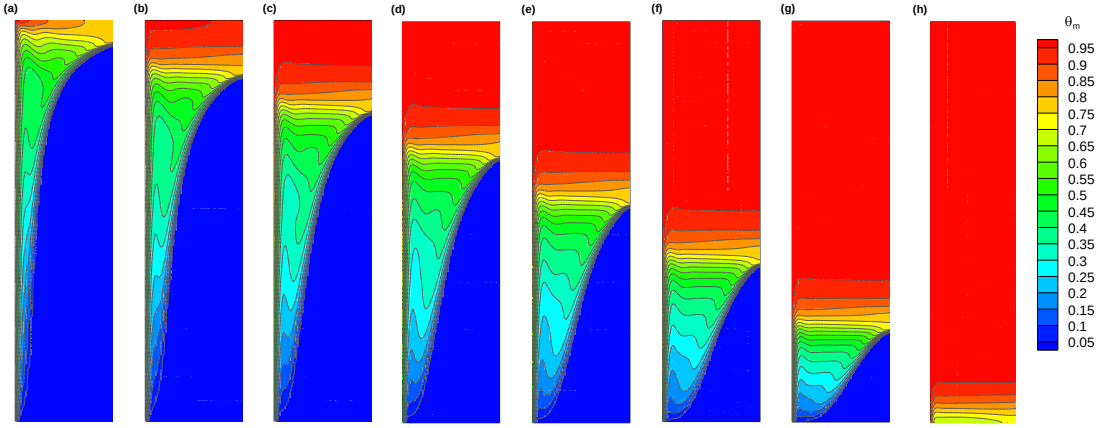

Figure 8: Isotherms for a downward HTF flow in channels at (a) $\tau = 5.45\times10^{-2}$, (b) 7.46×10^{-2}, (c) 9.466×10^{-2}, (d) 1.162×10^{-1}, (e) 1.377×10^{-1}, (f) 1.65×10^{-1}, (g) 1.98×10^{-1} and (h) 2.8×10^{-1}

3.2. Effect of the Reynolds number and HTF flow direction on the storage efficiencies

The effect of the Reynolds number on the time-wise variation of the sensible storage efficiency, for both HTF flow directions, is shown in Fig. 9. From this figure, it can be shown that, at the same moment and Reynolds number, the sensible storage efficiency is higher for a downward HTF flow direction. The difference of sensible storage efficiency between the both cases of HTF flow direction decreases as the Reynolds number augments. At the end of the charging process, the sensible storage efficiency reaches its maximum value and remains constant. For an upward HTF flow, the total charging time of LHSU is about $\tau =$ 0.3772, 0.3134 and 0.2448 for Re = 40, 100 and 2000, respectively. For a downward HTF flow, the charging time is $\tau = 0.308$, 0.2687 and 0.2206 for Re = 40, 100 and 2000, respectively. From these results, it can be concluded that the charging time of LHSU decreases with increasing Reynolds number. In other words, the sensible heat stored early in PCM for higher Reynolds number. In addition, the total charging time of LHSU is shorter for a downward HTF flow direction.

The effect of the Reynolds number on the time-wise variation of the latent storage efficiency is illustrated in Fig. 10. The results show that, for both HTF flow directions, the latent storage efficiency is higher for a large value of the Reynolds number. This behavior is mainly due to the fact that the increase in the Reynolds number intensifies heat transfer between HTF and PCM slabs and therefore accelerates the melting process. It is interesting to note that the latent storage efficiency is slightly higher for a downward HTF flow. But, as the melting process approaches to its end, the difference of latent storage efficiency between the both cases of HTF direction is gradually reduced to become virtually zero. For an upward HTF, the PCM is completely melted at $\tau =$ 0.2763, 0.2412 and 0.1984 for Re = 40, 100 and 2000, respectively. For a downward HTF flow, the PCM becomes completely melted at $\tau = 0.2735$, 0.2378 and 0.1958 for Re = 40, 100 and 2000, respectively. The

analysis of these results reveal that, for the mentioned values of the aspect ratio and Rayleigh number, the direction of HTF flow influences very slightly the melting time of PCM. However, the PCM is completely melted in a shorter time for higher Reynolds number. These results show that the increase in the Reynolds number reduced the time required for the complete melting of PCM. And the melting time is slightly lower for a downward HTF flow.

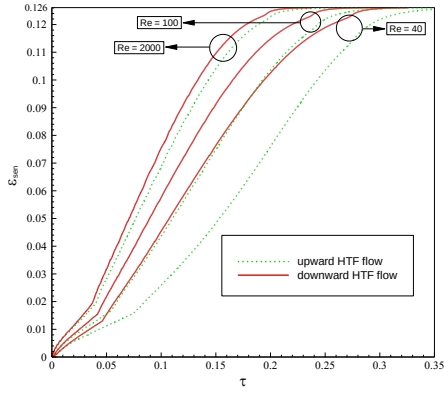

Figure 9: Effect of the Reynolds number on the sensible storage efficiency

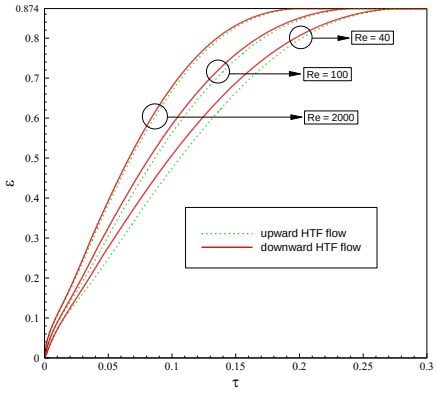

Figure 10: Effect of the Reynolds number on the latent storage efficiency

Conclusion

In the present study, a numerical analysis of the melting of PCM (Paraffin wax P116) in a rectangular latent heat storage unit heated by upward and downward HTF flows is conducted. A mathematical model based on the conservation equations of mass, momentum and energy has been developed to investigate the effects of the HTF flow direction and Reynolds number on the thermal performance and behavior of the storage unit. The results show that the increase in the Reynolds number enhances the heat transfer and leads to the decrease in the melting time of PCM. The results also reveal that the HTF flow direction strongly affects the sensible storage efficiency and, for all Reynolds numbers, the smallest charging time of LHSU (time when the sensible storage efficiency achieves its maximum) is obtained for a downward HTF flow.

Nomenclature

A	Aspect ratio, H/(d/2)
c	specific heat at constant pressure (J/kg K)
d	PCM slabs thickness (m)
D_h	hydraulic diameter (m), $D_h = 2w\ e/(w + e)$
$\bar{D}_h$	dimensionless hydraulic diameter
e	depth of the PCM slabs (e = 1 m)
f	liquid fraction
Fo	Fourier number, $Fo = t\ \alpha_{m,l}/ H^2$
k	conductivité thermique, (W/m/K)
$\bar{k}$	dimensionless thermal conductivity
l_0	characteristic length (m), $l_0 = \sqrt{Hd/2}$
$\dot{m}$	mass flow rate of HTF (kg/ s)
N	number of HTF channels
Pr	nombre de Prandtl
Ra	Rayleigh number
Re	Reynolds number
Ste	Stefan number
w	width of HTF channels (m)
$\bar{w}$	dimensionless width of HTF channels
X,Y	dimensionless Cartesian coordinates
U,V	dimensionless velocity components

Greek symbols

α	thermal diffusivity (m^2/s)
$\bar{\alpha}$	dimensionless thermal diffusivity
β	coefficient of thermal expansion (K^{-1})
θ	dimensionless temperature
τ	dimensionless time, $\tau = t\,\alpha_{m,l} / l_0^{\,2}$
μ	dynamic viscosity ($N\ s/m^3$)
ν	kinematic viscosity (m^2/s)
Δh	latent heat (J/ kg)
ρ	density (kg/ m^3)
ε	storage efficiency
ψ	stream function (m^2/ s)
Ψ	dimensionless stream function ,(= $\psi/\alpha_{m,l}$)

Subscripts

aver	average
e	inlet
f	heat transfer fluid (HTF)
l	liquid
lat	latent
m	phase change material (PCM)
melt	melting
o	outlet

s solid
sen sensible

References

[1] F. Kuznik, J. Virgone, Experimental assessment of a phase change material for wall building use, *Applied Energy*, volume 86, pages 2038-2046, 2009.
[2] W. Xiao, X. Wang, Y. Zhang, Analytical optimization of interior PCM for energy storage in a lightweight passive solar room, *Applied Energy*, volume 86, pages 2013-2018, 2009.
[3] C. Garnier, J. Currie, T. Muneer, Integrated collector storage solar water heater: Temperature stratification, *Applied Energy*, volume 86, pages 1465-1469, 2009.
[4] K. Sutthivirode, P. Namprakai, N. Roonprasang, A new version of a solar water heating system coupled with a solar water pump, *Applied Energy*, volume 86, pages 1423-1430, 2009.
[5] Z. D. Cheng, Y. L. He, J. Xiao, Y. B. Tao, R. J. Xu, Three-dimensional numerical study of heat transfer characteristics in the receiver tube of parabolic trough solar collector, *International Communications in Heat and Mass Transfer*, volume 37, pages 782-787, 2010.
[6] D. Brosseau, J. W. Kelton, D. Ray, M. Edgar, Testing of Thermocline Filler Materials and Molten-Salt Heat Transfer Fluids for Thermal Energy Storage Systems in Parabolic Trough Power Plants, *J. Sol. Energy Eng.*, volume 127, pages 8, 2005.
[7] Y.-L. He, J. Xiao, Z.-D. Cheng, Y.-B. Tao, A MCRT and FVM coupled simulation method for energy conversion process in parabolic trough solar collector, *Renewable Energy*, volume 36, pages 976-985, 2011.
[8] Y. B. Tao, Y. L. He, Numerical study on coupled fluid flow and heat transfer process in parabolic trough solar collector tube, *Solar Energy*, volume 84, pages 1863-1872, 2010.
[9] Z. Yang, S. V. Garimella, Molten-salt thermal energy storage in thermoclines under different environmental boundary conditions, *Applied Energy*, volume 87, pages 3322-3329, 2010.
[10] P. Charvát, L. Klimeš, M. Ostrý, Numerical and experimental investigation of a PCM-based thermal storage unit for solar air systems, *Energy and Buildings*, volume 68, Part A, pages 488-497, 2014.
[11] A. H. Mosaffa, C. A. Infante Ferreira, F. Talati, M. A. Rosen, Thermal performance of a multiple PCM thermal storage unit for free cooling, *Energy Conversion and Management*, volume 67, pages 1-7, 2013.
[12] M. Bechiri, K. Mansouri, Exact solution of thermal energy storage system using PCM flat slabs configuration, *Energy Conversion and Management*, volume 76, pages 588-598, 2013.
[13] J. P. A. Lopez, F. Kuznik, D. Baillis, J. Virgone, Numerical modeling and experimental validation of a PCM to air heat exchanger, *Energy and Buildings*, volume 64, pages 415-422, 2013.
[14] E. Halawa, W. Saman, Thermal performance analysis of a phase change thermal storage unit for space heating, *Renewable Energy*, volume 36, pages 259-264, 2011.
[15] W.-B. Ye, D.-S. Zhu, N. Wang, Fluid flow and heat transfer in a latent thermal energy unit with different phase change material (PCM) cavity volume fractions, *Applied Thermal Engineering*, volume 42, pages 49-57, 2012.
[16] M. Gharebaghi, I. Sezai, Enhancement of heat transfer in latent heat storage modules with internal fins, *Numerical Heat Transfer, Part A: Applications*, volume 53, pages 749-765, 2007.
[17] J. Borderon, J. Virgone, R. Cantin, Modeling and simulation of a phase change material system for improving summer comfort in domestic residence, *Applied Energy*, volume 140, pages 288-296, 2015.
[18] A. Lazaro, P. Dolado, J. M. Marín, B. Zalba, PCM–air heat exchangers for free-cooling applications in buildings: Experimental results of two real-scale prototypes, *Energy Conversion and Management*, volume 50, pages 439-443, 2009.
[19] H. El Qarnia, Theoretical study of transient response of a rectangular latent heat thermal energy storage system with conjugate forced convection, *Energy Conversion and Management*, volume 45, pages 1537-1551, 2004.
[20] H. Ait Adine, H. El Qarnia, Numerical analysis of the thermal behaviour of a shell-and-tube heat storage unit using phase change materials, *Applied Mathematical Modelling*, volume 33, pages 2132-2144, 2009.
[21] M. M. Prieto, B. González, Fluid flow and heat transfer in PCM panels arranged vertically and horizontally for application in heating systems, *Renewable Energy*, volume 97, pages 331-343, 2016.
[22] M. Bechiri, K. Mansouri, Analytical solution of heat transfer in a shell-and-tube latent thermal energy storage system, *Renewable Energy*, volume 74, pages 825-838, 2015.
[23] R. Elbahjaoui, H. E. Qarnia, M. E. Ganaoui, Melting of nanoparticle-enhanced phase change material inside an enclosure heated by laminar heat transfer fluid flow, *Eur. Phys. J. Appl. Phys.*, volume 74, pages 24616, 2016.

[24] R. Elbahjaoui, H. El Qarnia, Transient behavior analysis of the melting of nanoparticle-enhanced phase change material inside a rectangular latent heat storage unit, *Applied Thermal Engineering*, volume 112, pages 720-738, 2017.
[25] A. Laouadi, M. Lacroix, Thermal performance of a latent heat energy storage ventilated panel for electric load management, *International Journal of Heat and Mass Transfer*, volume 42, pages 275-286, 1999.
[26] W. M. Kays, M. E. Crawford, Convective Heat and Mass Transfer, McGraw-Hill, New York, 1970.
[27] A. D. Brent, V. R. Voller, K. J. Reid, Enthalpy-porosity technique for modeling convection-diffusion phase change: Application to the melting of a pure metal, *Numerical Heat Transfer*, volume 13, pages 297-318, 1988.
[28] J. M. Khodadadi, S. F. Hosseinizadeh, Nanoparticle-enhanced phase change materials (NEPCM) with great potential for improved thermal energy storage, *International Communications in Heat and Mass Transfer*, volume 34, pages 534-543, 2007.
[29] C. Gau, R. Viskanta, Melting and solidification of a metal system in a rectangular cavity, *International Journal of Heat and Mass Transfer*, volume 27, pages 113-123, 1984.
[30] O. Bertrand, B. Binet, H. Combeau, S. Couturier, Y. Delannoy, D. Gobin, M. Lacroix, P. Le Quéré, M. Médale, J. Mencinger, H. Sadat, G. Vieira, Melting driven by natural convection A comparison exercise: first results, *International Journal of Thermal Sciences*, volume 38, pages 5-26, 1999.